Preprints (www.preprints.org) | NOT PEER-REVIEWED | Posted: 7 February 2022 doi:10.20944/preprints202201.0446.v2

# Modeling the enhanced-efficacy and curing-depth of photo-thermal dual polymerization in metal (Fe) polymer composites for 3D printing

*Jui-Teng Lin[1,]*, Yi-Ze Lee[2], Jacques Lalevee[3]*

. [1] *New Photon Corp., New Taipei City, Taiwan; jtlin55@gmail.com*
. [2] *Department of Electrical and Engineering, National Taiwan University, Taipei, Taiwan; r09941019@g.ntu.edu.tw*
. [3] *Université de Haute-Alsace, CNRS, Mulhouse, France; jacques.lalevee@uha.fr*
.

**Abstract:** This article presents, for the first time, the efficacy and curing depth analysis of photo-thermal dual polymerization in metal (Fe) polymer composites for 3D printing of a 3-component (A/B/M) system based on the proposed mechanism of our group, in which the co initiators A and B are Irgacure-369, and charge-transfer complexes (CTC), respectively; and the monomer M is filled by Fe. Our formulas show the depth of curing (Zc) is an increasing function of the light intensity, but a decreasing function of the Fe and photoinitiator concentrations. Zc is enhanced by the additive [B] which produces extra thermal radical for polymerization under high temperature. The heat (or temperature) increase in the system has two components : (i) due to the light absorption of Fe filler, and (ii) heat released from the exothermic photopolymerization of the monomer. The heat is transported to the additive (or co-initiator) [B] to produce extra radical R' and enhance the monomer conversion function (CF). The Fe filler leads to temperature increase, but also limits the light penetration leading to lower CF and Zc, which could be overcome by the additive initiator [B] in thick polymers. Optimal Fe for maximal CF and Zc are explored theoretically.

. **Keywords:** polymerization kinetics; monomer conversion; metal composited; 3 D printing; additive manufacturing.
.

---

## 1. Introduction

To overcome the poor mechanical properties of pure polymers, metal polymer composites (MPCs) combine the functionalities of metals and the advantages of polymers have been proposed. [1-7] However, MPCs are still suffer some problems such as extremely poor metal-polymer compatibility, high metal filler content, and functional singularity.[8-10]

Light emitting diodes (LED) photoinitiated polymerization offer many advantages such as its solvent-free formulation, mild conditions (ambient temperature, without monomer purification or stabilizers removal etc.), fast reaction rates, and in line with the green chemistry. [11-15] Copper complex photoredox catalyst photocatalyst have been reported by our group for free radical/cationic hybrid photopolymerization.[16,17] Nevertheless, very few polymeric composite containing metal fillers are prepared by the photopolymerization process due to the poor light penetration depth which also limits the curing dept. We have recently reported TMPTA as the model monomer, iron powder as filler and Irgacure 369 (Irg 369) as photoinitiator with the aid of two charge-transfer complexes (CTCs) as dual thermal/photochemical initiators uisng LED at 405 nm, in which the lack of light penetration was indirectly overcome with the help of CTC in association with heat release during the radical photopolymerization.[18,19] In the dual thermal/photo polymerization process, we

Preprints (www.preprints.org) | NOT PEER-REVIEWED | Posted: 7 February 2022 doi:10.20944/preprints202201.0446.v2



have sucessfully achieved 10 times more dpeth of curing than that of photopolymerization alone.

In supporting our recent measured data, Bonardi et al [17] and Ma et al. [18,19], this article will present the kinetics, the conversion profiles features and the depth of curing of a 3-component (A/B/M) system based on the proposed mechanism of our group.[19] We will demonstrate that the conversion function (CF) has two opposite trends in their time profiles depending on the amount of Fe. This switching feature predicted by our formula is also justified by our measured data. Analytic formulas for the CF, depth of curing and heat (temperature) profiles will be derived rigorously.

## 2. Methods and Modeling Systems

### 2.1. Photochemical Kinetics

In association with the proposed scheme of our group published in Ma et al [19], we propose in Figure 1, a 3-component system (A/B/M) defined by the co initiators [A] and [B] with monomer (M), in which the initiator [A] is excited to its first-excited state A*, and a triplet excited state T having a quantum yield (q). The triplet state T interacts with [A] to produce radical (R) which couple with M for photopolymerization and release heat (H). Additional heat (H) is produced by the UV light absorption of the filler, iron mixed in the monomer. Heat is also produced by the light absorption of the iron filled in the monomer. The heat is transported to the additive (or co-initiator) [B] to produce extra radical R'. Therefore, the polymerization can be induced by the photo-radical (R) and enhanced by the thermal-radical (R'). A specific measured system related to Figure1 was reported by Ma et al [19] for a 3-component system of PI/B/M, where PI is the photoinitiator Irgacure 369, B is a co-initiator of charge-transfer complex (CTC), and the M is the monomer rimethylolpropane triacrylate (TMPTA), which is filled with filler iron (Fe).

A second example was proposed by our group published in Bonardi et al [17], in which A is an absorbing phosphine dye of an infrared light, B is an iodonium salt as the co-initiator, and BlocBuilder MA is the thermal initiator. The light heating in the system of Ma et al is due to the light absorption of Fe filler in the monomer TMPTA, whereas it is due to the direct light absorption of the thermal initiator in the second example. In both systems, the heat (or temperature increase) in the monomer has two components: the light heater and the heat released from the exothermic photopolymerization of the monomer.

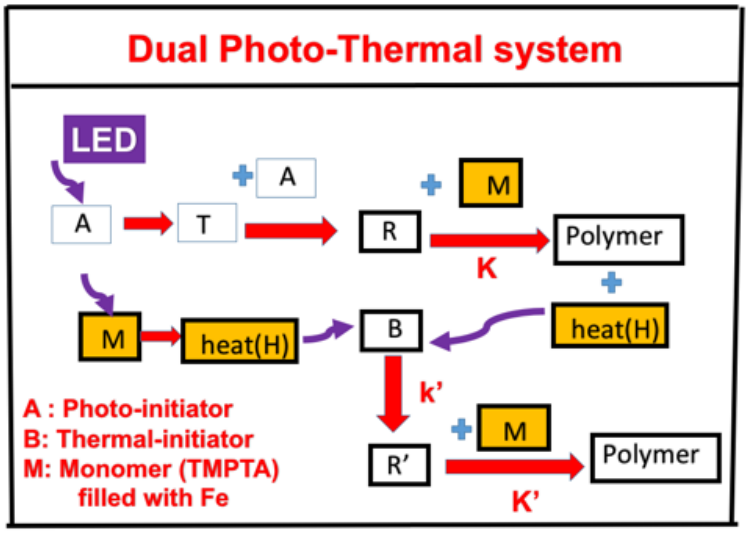


**Figure 1.** The schematics of a dual function system, (A/B/H), The heat (H) can be produced by the light absorption of the iron filled in the monomer (M) and the heat released by the

Preprints (www.preprints.org) | NOT PEER-REVIEWED | Posted: 7 February 2022 doi:10.20944/preprints202201.0446.v2



photopolymerization, in which R and R' lead to a photo-thermal dual polymerization (see text for more details).

The kinetic equations for our previous systems [20-22] are revised for the new system of Figure1 (A/B/H/M) as follows. We will use the short hand notations for the concentrations: [A] for photoinitiator Irgacure 369, [B] for the additive CTC, F for the filler iron (in wt%), R and R' for the photo and thermal radical, respectively.

$$\frac{d[A]}{dt} = -bI[A] + REG \quad (1)$$

$$\frac{d[B]}{dt} = -k'(t)[B] \quad (2)$$

$$\frac{dT}{dt} = bI[A] - (K'' + k[A] + k''M + P'[O_2])T \quad (3)$$

$$\frac{dR}{dt} = k[A]T - KMR - P[O_2]R - VR^2 \quad (4)$$

$$\frac{dR'}{dt} = k'(t)[B] - K'MR' \quad (5)$$

In Equation (3) and (4) we have also included the ogygen inhibition effects (OIH), the $P(z)[O_2]$ term with $P(z)= P_0 \exp(-Dz)$, and D is the oxygen diffusion constant. We note that the OIH reduces the active radical (R) leading to a delayed rising profile of the conversion efficacy for systems in air. [23] P'(z) has the similar z dependence as that of P(z), i.e., near the sample surface (with small z) has higher OIH than large depth.
In Equation (2) ans (5), k'(t) is the time-dependent decompisition rate of B to produce thermal radical R', given by an Arhennius formula k'(t)=f exp[-Ed/(rH(t)]; f is the frequency factor for thermal initiator decomposition and Ed is the activation energy, r is a gas constantant. H is the heat (or temperature) in the monomer due to two components: (i) the aFI(z,t) term, due to light absorption of iron filler given by the absorption constant (a), light intensity (I) and iron concentration (F); and (ii) the heat released from the exothermic photopolymerization of the monomer (the KMR term), and (iii) the heat transport to the co-initiator, B. Therefore, H is given by a generalized heat diffusion equation

$$\frac{dH(z,t)}{dt} = aFI(z,t) + KRM - b'H + c\nabla^2 H \quad (6)$$

where b' is the heat transport constant, the last term is the thermal conduction term in depth(z). The UV light intensity has the depth (z) dependence due to the absorption of PI, [A], and iron filler (F) given by

$$\frac{dI(z,t)}{dz} = -(b[A] + aF)I(z,t) \quad (7)$$

The monomer (M) conversion rate equation has three components: triplet state (T) direct coupling,
Under the above quasi-steady-state solutions and for unimolecular case for R, we obtain the simplified equations (with the thermal conduction term ignored) as follows.

$$\frac{d[A]}{dt} = -(bI[A] - REG) \quad (8)$$

$$\frac{d[B]}{dt} = -k'(t)[B] \quad (9)$$

$$\frac{dH}{dt} = aFI + k[A]T - b'H \quad (10)$$

Preprints (www.preprints.org) | NOT PEER-REVIEWED | Posted: 7 February 2022 doi:10.20944/preprints202201.0446.v2



The conversion efficacy (CF) defined by CF=1 - $M(t)/M_0$, with M(t) given by the solution of

$$\frac{dM}{dt} = -[k''M + k[A]/(1 + OIH)]\,T - k'[B] \qquad (11)$$

## 3. Methods and Results

A full numerical simulation is required for the solutions of Equation (9) to (12), which will be presented elsewhere. We will focus on comprehensive analysis for special features and the key factors of dual radical enhancement for efficient conversion related to the measured data of Ma et al [19], based on the analytic formulas to be derived as follows.

### 3.1 Analytic results

In general, Equation (11) and (12) require numerical simulation. For analytic formulas, we further approximate g=(1-D)/(k[A]), with D(t)=k''M(t)/(k[A]) being the second-order corection term, such that T=bI(1-D)/(k[A]), Equation (11) and (12) are reduced to

$$\frac{dH}{dt} = (aF + b)I(z,t) - b'H - bD(t)I(z,t) \qquad (12)$$

$$\frac{dM}{dt} = -[1/(1 + OIH) + (k''/k)M/[A]](1 - D)\,bI(z,t) - k'(t)[B] \qquad (13)$$

Analytic formulas need further assumption of RGE is taken as a mean reduction factor (f'), such that bI[A]-RGE = f'bI[A] having a value of f'=0 to 1.0. The first-order solution of Equation (9) is given by $[A]=A_0 \exp(-dt)$; with d=bI(z), for f'=1, and I(z,t) assumed to be time-independent, that is the increase of I(z,t) due to the depletion of [A] is neglected. For the perfect recycle case, f=0, and $[A] = A_0$ is a constant. Using an average of [A(z,t)] over z and t (defined as A'), we obtain $I(z)=I_0 \exp[-Gz]$, with G=aF + bA'.

$$H(z,t)= H_0 \exp(-b't) + (d'/b')[1-\exp(-b't)] - Q(t) \qquad (14)$$

where $H_0$ is the initial value of H(t=0), and $d'=(aF+b)I(z)= (aF+b)I_0 \exp[-Gz]$. We have also added a correction factor $Q(t)=k''M_0/(kA_0)\,[1-\exp(-D't)]D'=qt$ (for small t), with D'=1+k''. We note that H(t) has a transient state value $H_0$ (1-b't) + (d'-q)t, and a steady state value (aF+b)I(z)/b'. Moreover, for z>0, d' has an optimal value at F=F*, and it is a decreasing function of F, for F>F*. This optimal value is due to the competing term (aF) in $d'=(aF+b)I_0 \exp[-(aF+bA')]$. Therefore, a higher F>F* and/or A' leads to less light penetration due to the absorption factor G=aF+bA' in $I(z) =I_0 \exp[-Gz]$, and also leads to lower heat released (temperature) in the monomer, H(t).

Using Equation (15) to solve for Equation (10), with appromximated $k'(t)=f \exp[-Ed/(rH(t)]=f[1- Ed/(rH(t)]=f[1- (1-Q't)Ed/(rH_0)]$, with $Q'=(d'-q)/H_0 -b'$, we obtain

$$[B](z,t)= B_0 \exp[-P(t)] \qquad (15)$$

where $P(t)=f(P'+0.5P''t)t$, with $P'= 1- Ed/(rH_0)$, $P''= Ed/(rH_0)Q'$.

Using the first-order solution of Equation (14), with D=OIH=k'(t)=0, and $M(t)=M_0 \exp(-k''dt)$ and $[A]=A_0 \exp(-dt)$, with d=bI, we find the second-order solution (including k'[B]) of Equation (14) given by

.

$$M(t)=M_0 -[dt+(k''/k)(M_0/A_0)V(t)] - k' B_0V'(t) \qquad (16)$$

Preprints (www.preprints.org) | NOT PEER-REVIEWED | Posted: 7 February 2022 doi:10.20944/preprints202201.0446.v2



where V(t)=[1- exp(-st)]/s, with s=(1+k")bI; V'(t)=[1- exp(-fP't)]/(fP'), with P'=1- Ed/(r$H_0$).

Two special cases are analyzed for Equation (17) as follows.

(a) For steady-state: V(t)=1/s, V'(t)=1/(fP'), we obtain the conversion efficacy (CF) defined by CF=1-M(t)/$M_0$,

$$CF(z,t)= bIt/M_0+k''/[(1+k'')kA_0] + k' B_0/(fP'M_0) \quad (17.a)$$

We note CF is proportional to the light dose (It) that this feature is only for the case of unimolecular termination of the radical R which is proportional to (bI). For the case of bimolecular [20], R is proportional to the power of $(bI)^{0.5}$, and the steady-state value of CF is proportional to $(bI)^{-0.5}$.

(b) For transient state, V(t)=V'(t)= t, we obtain the CF

$$CF(z,t)= b(It)[1/M_0 + k''/(kA_0)] + k'tB_0/M_0. \quad (17.b)$$

We note that Equation (18) has 3 terms proportional to the light dose E=I(z)t, and initial concentrations $1/A_0$, $1/M_0$, and $B_0$ and the absorption constants, b. However CF (for z>0) is a decreasing function of Fe, since I(z) =$I_0$ exp[-(aF+bA')z].

### 3.2 Depth of Curing (DoC)

As shown by Equation (7) the light intensity is an exponentially decreasing function of the depth(z) according to a Beer-Lambert law (BLL). However, for the situation of time-dependent intensity I(z,t) due to the depletion of the PI concentration, A(t)=$A_0$ exp(-dt), a generalized BLL was developed by Lin [20], such that the solution of Equation (8) becomes I(z,t)=$I_0$ exp[-Gz], in which G is an average of [A(z,t)] over z and t (defined as A'), given by G=aF + bA'.

A curing depth ($Z_C$) is defined by when the conversion efficacy is higher than a critical value, CF>C*. Using I(z,t)= $I_0$ exp[-Gz], and Equation (18) for CF, we obtain

$$Z_C = \ln[(SI_0)/(C^* - S')\,]/(aF + bA') \quad (18.a)$$

where S= bt[1/$M_0$ + k"/(k$A_0$)]; and the enhancement factor, S' = k't($B_0H_0$)/$M_0$.
We note that $Z_C$ is proportional to the light dose $I_0$t, but it is a decreasing function of the effective absorption constant (aF+bA'), with A' being the z and time -averaged PI concentration [A], given by A'. Equation (19) show that Zc is enhanced by the additive [B] via S' = k't($B_0H_0$)/$M_0$, which is proportional to k'$B_0H_0$, i.e., the limited light penetration due to Fe is overcome by the additive CTC, or [B]. Equation (19) shows that Zc is proportional to ln($SI_0$) under the unimolecular case, with neglected $VR^2$ term in Equation (4). For the bimolecular dominant case (with $VR^2$ >>KRM), Equation (19) is revised to [21]

$$Z_C = 2\ln[S{I_0}^{0.5}/(C^* - S')\,]/(aF + bA') \quad (18.b)$$

We note that more detailed discussion and numerical results of Zc and curing time maybe found in our previous work. [20,22]

As shown by Equation (15), when Fe is too high the DoC is too low to create effective polymerization and it is limited to thin films. For lower Fe of 10% to 30%, the DoC is larger than the sample thickness and sharp edges are produced. Moreover, high Fe leads to strong

Preprints (www.preprints.org) | NOT PEER-REVIEWED | Posted: 7 February 2022 doi:10.20944/preprints202201.0446.v2



light absorption and the light dose is smaller than the polymerization threshold at certain sample depth.

### 3.3 General features and new findings

As shown by Eqs. (9) to (18), the following significant features of the [A]/[B]/M system which was also proposed by Ma et al [19]). Our modeling has explored the follow general features, in which some new findings are not yet explored in our previous experiment of Ma et al [23], but might be justified in our future works.

(i) As shown by Equation (6), the heat (or temperature) increase in the system has two components: (a) the aFI(z,t) term, due to light absorption of iron filler given by the absorption constant (a), light intensity (I) and iron concentration (F); and (b) the heat released (the KMR term) from the exothermic photopolymerization of the monomer.

(ii) The solution of heat H(t) given by Equation (14) has two terms which has opposite trends in their time profiles; the first term is a decaying function, whereas the second term is an increasing profile. We note that H(t) has a transient state value $H_0$ (1-b't) + d't, and a steady state value (aF+b)I/b'. Therefore, for F>F*, higher F and/or A' leads to less light penetration due to the term G=aF+bA' in I(z) =$I_0$ exp[-Gz], and lower heat released (temperature) in the monomer. This feature of optimalization is valid only for z>0. It does not exist for surface (with z=0). Numerical simulation will be shown later for this optimal feature.

(iii) As shown by Equation (8) and (12), (14), the monomer conversion has 3 components: (a) from the direct coupling of T and [A], (b) the coupling of photon-radical (R) with M, and (c) coupling of thermal-radical (R') and M; in which R' is an enhancement radical produced from the co-initiator, [B], under a high temperature given by the heat function, H(t). We note that the Fe filler leads to temperature increase, but also limits the light penetration, leading to lower CF and DoC, which could be overcame by the additive initiator [B] for thick samples.

(iv) As shown by Equation (17) has terms proportional to the light dose E=It, and initial concentrations $A_0$, $H_0$ and the last term of Equation (17), k'$B_0$/$M_0$, which is the enhancement factor in the presence of co-initiator B. Above features are for the case with unimolecular coupling of KRM term in Equation (4). For the situation of a strong bimolecular termination, we need to include the coupling of $VR^2$ in Equation (4), and leading a CF which is proportional to the $(bI)^{0.5}$ (for transient state); and inverse proportional to $(bI)^{-0.5}$ at steady-state, i.e., higher intensity leads to a lower steady-state CF than lower intensity. The enhancement factor is given by S' = k't($B_0H_0$)/$M_0$, shown in Eqs. (17) and (18). The CF enhancement in the presence of co-initiator B was also reported experimentaly by Bonardi et al. [17]

(v) As show by Equation (19), the depth of curing (DoC), Zc, is an increasing function of the light intensity. However, there is an optimal Zc, based on the parameter of (aF+b), i.e., there is an optimal value of the iron concentration (F) which can be found mathematically by taking the derivative of Zc over d', and let it equal 0, which can be also found numerically [20]. This optimal value is due to the competing term in d'=(aF+b)$I_0$ exp[-(aF+A')]. The enhanced Zc is given by S' = k't($B_0H_0$)/$M_0$. Equation (18) also defines the minimal enhancement factor (S*) to reach a sample depth of Z' given by the condition of when (aF+b)Z'>ln ($SI_0$/(C*-S'), or S'> S*, with S*=C*- $SI_0$ exp[-(aF+b)Z'], or k't($B_0H_0$)/$M_0$>C*-$SI_0$ exp[-(aF+b)Z'].

(vi) Our modeling also shows that there is an optimal condition for the initiator PI concentration given by d(CF)/dF=0, with CF given by Equation (17), which also requires numerical stimulation. [20]

### 3.4 Theoretical predictions and future directions

Preprints (www.preprints.org) | NOT PEER-REVIEWED | Posted: 7 February 2022 doi:10.20944/preprints202201.0446.v2



Based on our analytic formulas, Equation (14), we show, in Figure 2, the volume (at z=1.0cm) temperature profiles in the monomer in the absence of PI (with b=0), with heat produced by light absorption of Fe only (or b=0). It shows that larger Fe mixed in the monomer leads to lower temperature profiles deu to the light penetration depth decreases as shown by $I(z,t)=I_0 \exp(-Gz)$, with G=aF + bA', which is a strong decreasing function of G. The saturation is due to the heat transport term, b'H.

Figure 3 shows the temperature profiles (at z=1.0 cm) in the presence of co-initiators, [A] and [B], with $aFI_0$ = (0, 0.1, 0.2) (1/sec), for a fixed $bI_0$=10 (1/sec), shown by curves (1,2,3) which have much higher temperature than the case of pure Fe absorption (with b=0), curve-4, Curves 1 to 3 also have much faster increasing profiles due to the strong heat transport term of b'H (with b'=0.035), comparing to the weak coupling curve-4 (with b'=0.002). The drop of Curves 1 to 3 is due to Q(t)=qt in Eq. (14), with q=1.5 for Figure 3.

Based on our formula, Equation (18), we also show, in Figure 5, the DoC (Zc) as the function of various parameters. Figure 4(A) shows that Zc is an increasing function of S', the enhancement factor given by $S' = k't(B_0H_0)/M_0$, for a given curing threshold C*=0.4, and fixed $SI_0$=0.7, aF+bA'=1.0. Figure 5(B) shows that Zc is a decreasing function of the factor (aF+bA'), Figure 5(C) shows that Zc is an increasing function of $SI_0$, which is proportional to the light dose $tI_0$, and the coupling constant, b, as shown by Equation (19).

Figure 4 shows the optimal feature for a maximal heat produced by the light absorption of Fe, based on Equation (14). The optimal feature exists only for z>0, due to the light intenisty given by $I(z,t)=I_0 \exp(-Gz)$, with G=aF + bA', which is a strong decraesing function of (aF+bA'), for z>0. These features are show in Figure 4, for z=(0, 0.4, 0.5, 0.6) cm.

Based on our modleing predictions described above, we propose to conduct the following new measurements, whcih are not yet explored in Ref. [24].

(i) CF profiles for various initiator concentrations, $A_0$ and $B_0$, to justify our predicted enhancement factor give by S, in Equation (14) and (18).

(ii) CF profiles for various light intensity ($I_0$) to justify the steady-state CF scaling law of $(bI_0)^m$, with m=1.0 and -0.5;

(iii) curing depth (Zc) for various enhanced factor given by $S'=k't(B_0H_0)/M_0$, as shown by Figure5.

(iv) the optimal feature shown by Figure4, for various $aFI_0$, for a maximal heat produced by the light absorption of Fe.

Besides the enhancement effects discussed in the present article using an additive of CTC, there are many other strategies have been reported by our group, including the use of multi-wavelength light and strategies of reduction the oxygen inhibition.[24-28] A critical review for photopolymerization for 3D bioprinting can be found in Ref. [24].

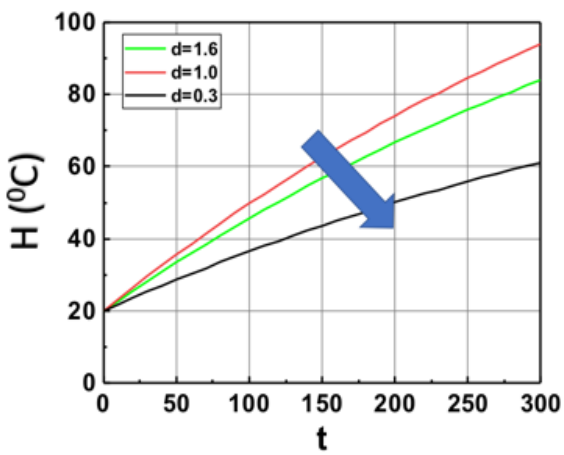

Preprints (www.preprints.org) | NOT PEER-REVIEWED | Posted: 7 February 2022 doi:10.20944/preprints202201.0446.v2



**Figure 2.** The calculated temperature (at z=1.0 cm) profiles of monomer based on Equation (15) for various weight concentration of Fe, with $aFI_0$ = (0.3, 1.0, 1.6) (1/sec) and b'=0.002 (1/s), in the absence of PI (with b=0), with heat produced by light absorption of Fe only, with inutial gemperature $H_0$=20 $^0$C.

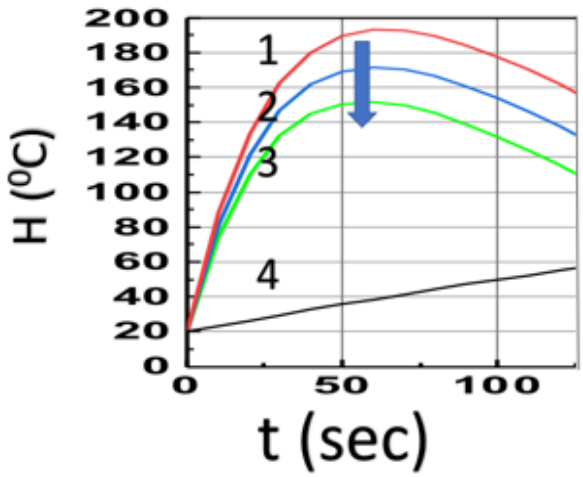


**Figure 3.** Same as Figure 2, but in the presence of co-initiators, [A] and [B]. with $aFI_0$= (0, 0.5, 1.0, 1.5) (1/sec), for Curves 1,2,3 (with $bI_0$ =10), and Curve-4 in the absence of PI (with b=0).

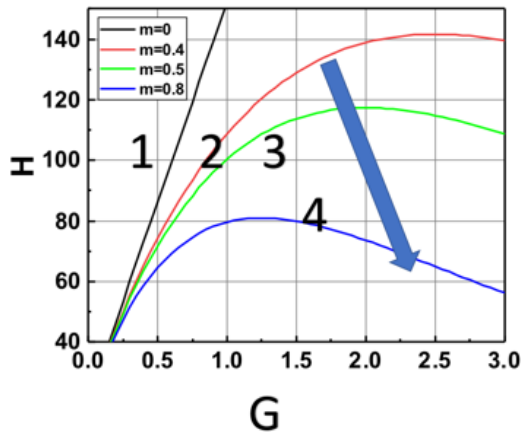


**Figure 4.** The calculated temperature of monomer versus G =aF + bA' based on Equation (15) at various sample depth z=(0, 0.4, 0.5, 0.6) cm, for curves (1,2,3,4), at t=200 sec.

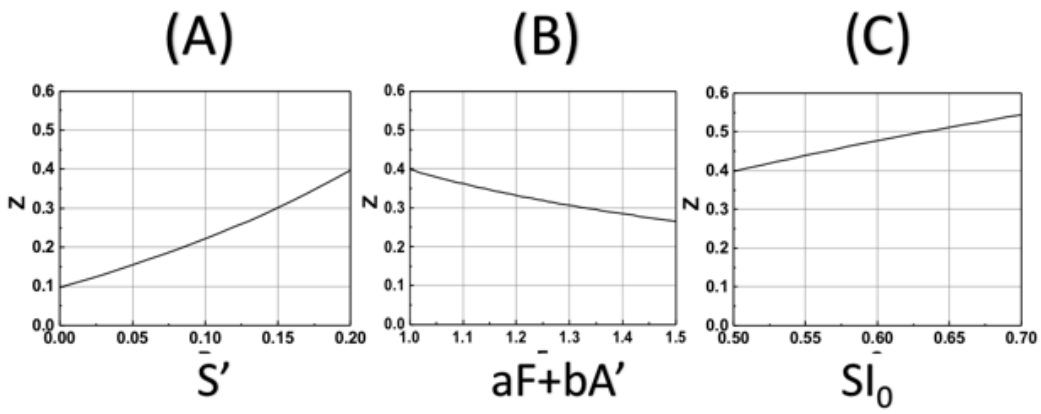

Preprints (www.preprints.org) | NOT PEER-REVIEWED | Posted: 7 February 2022 doi:10.20944/preprints202201.0446.v2



**Figure 5.** The calculated DoC (Zc) based on Equation (19) for various parameters: (A) for Zc vs S' with fixed $SI_0$=0.7, aF+bA'=1.0 and C*=0.4; (B) for Zc vs aF+bA', with fixed $SI_0$=0.5 and S'=0.5; (C) for Zc vs $SI_0$=0.5, with fixed and S'=0.2 and aF+bA'=1.0.

### 3.5 Analysis of measured data

The measured data are shown in Figure6 of our group, Ma et al [19], in which a PI Irgacure 369 is exposured to a LED at 405 nm (0.11 W $cm^{-2}$) for various iron (Fe) concentrations.

Figure 6 (A) shows the measured conversion profiles of TMPDA for various Fe concentrations. These profiles can be analyzed by our CF shown in Equation (18), which shows a typical saturation profile defined by Q'(t)=[1- exp(-b't)]/b' in Equation (17).

Figure 6 (B) shows the measured DoC for various Fe concentrations. These profiles can be analyzed by our Zc shown in Equation (19), which shows Zc is an increasing function of the light intensity $I_0$, but a decreasing function of the Fe (F) and PI concentration (A'), shown by the term (aF+bA'). The DoC is enhanced by the additive [B] via the S function which is proportional to (bt)[(1/$M_0$ - $A_0$) + k'$B_0$/(b'$M_0$)]. Our measured data had yielded (10 times) thick composites under the same dose using a LED irradiation at 405 nm.

Figure 6 (C) shows the temperature profiles in the absence of PI. They are related to the Equation (12) and (14) with b=0, but b'>0. This feature is also predicted by our theory as shown in Figure 2.

Figure 6 (D) shows the temperature profiles for various Fe concentrations. These profiles can be analyzed by Equation (14), which shows that H(t) has a transient state value $H_0$ (1-b't) + d't, and a steady state value d'/b', with d'=(aF+b)I(z), with I(z) = $I_0$ exp[-Gz]. Therefore, higher F and/or A' leads to less light penetration due to the absorption factor G=aF+bA', and also leads to a lower heat released (temperature) in the monomer, as shown by the measure curves of Figure 6 (D). These features are also predicted by our theory as shown in Figure 3. The CF enhancement in the presence of co-initiator B was also reported by Bonardi. [17]

We found that wt10% and wt30% Fe filler resin can achieve perfect three-dimensional structure, as shown in Figure 7A and B, with great spatial resolution for the photoproducts in the presence of the iron fillers. However, when the content of iron keeps up to 50% wt%, the pattern was not flat and some area under irradiation wasn't be fabricated (Figure 7C). See more detailed of measurement method in Ref. [19].

Preprints (www.preprints.org) | NOT PEER-REVIEWED | Posted: 7 February 2022 doi:10.20944/preprints202201.0446.v2



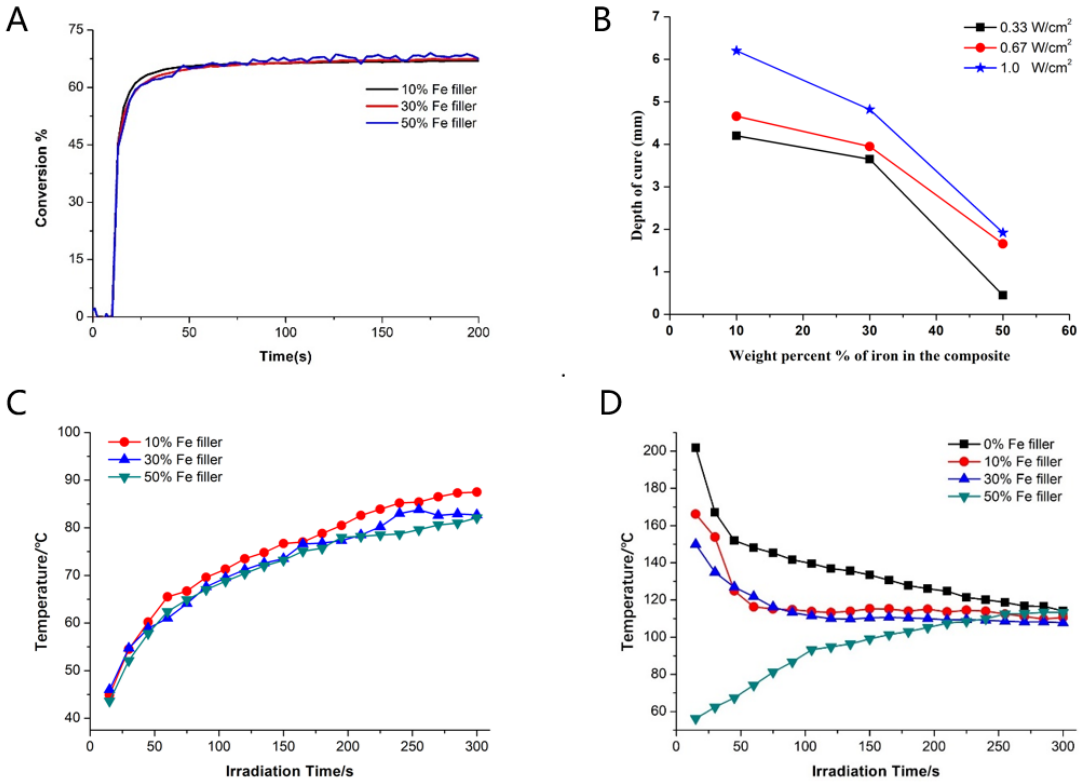


**Figure 6** (A) Measured photopolymerization profiles of TMPTA in laminate (25 µm thickness) initiated by Irgacure 369 upon exposure to LED@405 nm in the presence of Fe filler with different contents (wt%); (B) DoC results for the iron filler-based composites under the irradiation of high power LED@405 nm (0.33 W $cm^{-2}$; 0.67 W $cm^{-2}$; 1.0 W $cm^{-2}$); (C) temperature profiles of TMPTA with various wt% Fe in the absence of Irgacure 369; (D) temperature profiles of TMPTA with various wt% Fe in the presence of Irgacure 369 ($2.5\times10^{-5}$ mol $g^{-1}$ TMPTA). After Ma et al. [19]

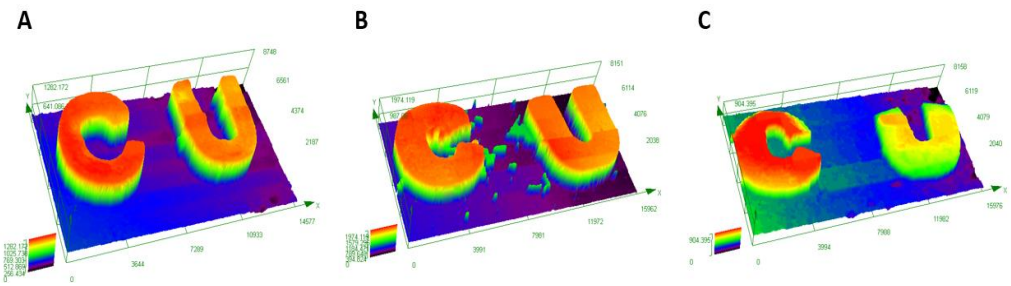


**Figure 7.** Optical microscopy of the 3D patterns printed from TMPTA containing: (A) 10% wt%, (B) 30% wt%, and (C) 50% wt% content of iron filler; All printing experiments were performed with $5.5*10^{-5}$ mol/g CTC(EMIM) in TMPTA. The scale bar is 2000 µm. After Ma et al. [19]

## 4. Conclusions

We have demonstrated theoretically and justified by measured CF profiles of a 3-component (A/B/M) system based on the proposed mechanism of our group, Ma et al [19], in which the co initiators are A, Irgacure 369, and B, charge-transfer complexes (CTC), and the monomer M is TMPDA. Our formula show the depth of curing (Zc) is an increasing function of the light intensity, but a decreasing function of the Fe and photoinitiator concentration. Zc is enhanced by the additive [B] which produces extra thermal radical for polymerization

under high temperature. The heat (or temperature) increase in the system has two components: due to light absorption of iron filler, and heat released from the exothermic photopolymerization of the monomer. The heat is transported to the additive (or co-initiator) [B] to produce extra radical R' and enhance the monomer conversion function (CF). For small Fe concentration (F), the CF is given by a decaying function; whereas for large F, it is given by a time increasing profile, The switching profile from a time decaying one (for small F) to a time growing profile (for large F) were also shown by the measured curves of Figure 2(D). This is a rather surprising feature predicted by our formula and justified by our measured data.[19]

**Acknowledgments:** JTL thanks the internal grant of New Photon Corp. JL thanks the the Aix Marseille University and The Centre 55 National de la Recherche (CNRS) for financial support.

Conflicts of Interest: JT Lin is the CEO of New Photon Corp.

References

1. D.K. Patel, A.H. Sakhaei, M. Layani, M, Highly Stretchable and UV Curable Elastomers for Digital Light Processing Based 3D Printing, Adv. Mater. 2017, 29, 1606000.
2. B. Narupail, A. Nelson, 100th Anniversary of Macromolecular Science Viewpoint: Macromolecular Materials for Additive Manufacturing, ACS Macro Letters, 2020, 9, 627-638.
3. Z. Xu, C. Gao, In situ Polymerization Approach to Graphene-Reinforced Nylon-6 Composites, Macromolecules, 2021, 43, 6716-6723.
4. Y. Zhang, L. Josien, J.P. Salomon, A. Simon-Masseron, J. Lalevée, Photopolymerization of Zeolite/Polymer-Based Composites: toward 3D and 4D Printing Applications, ACS Applied Polymer Materials, 2021, 3, 400-409.
5. Y. Zhang, L. Josien, J.P. Salomon, A. Simon-Masseron, J. Lalevée, Radical photoinitiation with LEDs and applications in the 3D printing of composites, Chem. Soc. Rev. 2021, 50, 3824-3841.
6. Liu, Y.; Lin, Y.; Jiao, T.; Lu, G.; Liu, J. Photocurable modification of inorganic fillers and their application in photopolymers for 3D printing, Polym. Chem. 2019, 10, 6350-6359.
7. Y. Xin, H. Peng, J. Xu, J. Zhang, Ultrauniform Embedded Liquid Metal in Sulfur Polymers for Recyclable, Conductive, and Self-Healable Materials, Adv. Funct. Mater. 29(17) (2019) 1808989.
8. Z. Lei, P. Wu, A supramolecular biomimetic skin combining a wide spectrum of mechanical properties and multiple sensory capabilities, Nature Communications 9(1) (2018) 1134.
9. S. Dadashi-Silab, S. Doran, Y. Yagci, Photoinduced Electron Transfer Reactions for Macromolecular Syntheses, Chem. Rev. 2016, 116, 10212-10275.
10. N. Corrigan, N. Yeow, J. Judzewitsch, P. Xu, C. Boyer, C. Seeing the Light: Advancing Materials Chemistry through Photopolymerization, Angew Chem Int Ed Engl. 2019, 58, 5170-5189.
11. P. Garra, A. Caron, A. Mousawi, B. Graff, B. Morlet-Savary, J. Lalevée, Photochemical, Thermal Free Radical, and Cationic Polymerizations Promoted by Charge Transfer Complexes: Simple Strategy for the Fabrication of Thick Composites, Macromolecules, 2018, 51, 7872-7880.
12. P. Garra, F. Dietin, B. Morlet-Savary, F. Dumur, J. Lalevée, Photopolymerization processes of thick films and in shadow areas: a review for the access to composites, Polym. Chem. 2017, 8, 7088-7101.

13. Y. Xu, Z. Ding, H. Zhu, Y. Zhang, S. Knopf, P. Xiao, J. Lalevée, Preparation of Iron Filler-Based Photocomposites and Application in 3D Printing, Macromolecular Materials and Engineering 2021, 306, 2000720.
14. P. Garra, F. Dietin, B. Morlet-Savary, F. Dumur, J. Lalevée, Charge Transfer Complexes as Pan-Scaled Photoinitiating Systems: From 50 µm 3D Printed Polymers at 405 nm to Extremely Deep Photopolymerization (31 cm), Macromolecules, 2018, 51, 57-70.
15. H. Mokbel, D. Anderson, R. Plenderleith, F. Dietlin, F. Dumur, J. Lalevée, Copper photoredox catalyst "G1": A new high performance photoinitiator for near-UV and visible LEDs. J. Polym. Chem. 2017, 8, 5580–5592.
16. H. Mokbel, D. Anderson, R. Plenderleith, F. Dietlin, F. Dumur, J. Lalevée, Simultaneous initiation of radical and cationic polymerization reactions using the "G1" copper complex as photoredox catalyst: Applications of free radical/cationic hybrid photopolymerization in the composites and 3D printing fields. Prog. Org. Coat., 2019, 132, 50–61. DOI: 10.1016/j.porgcoat.2019.02.044.
17. A. H. Bonardi, F. Bonardi, G. Noirbent, F. Dumur, D. Gigmes, J. Lalevee, Free-Radical Polymerization upon Near-Infrared Light Irradiation, Merging Photochemical and Photothermal Initiating Methods. Journal of Polymer Science, 2020, 58, pp.300- 308. ff10.1002/pol.20190079ff.
18. Q. Ma, S. Liu, M. Le Dot, H. Mokbel, Y. Zhang, B. Graff, J. Lalevée, Imidazole based dual photo/thermal initiators for highly efficient radical polymerization under air with a metal-free approach, Polym. Chem. 2021, 12 6386-6391.
19. Q. Ma, Y. Zhang, A. Lunay, M. Le Dot, S. Liu, J. Lalevée, How to overcome the light penetration issue in photopolymerization? An example for the preparation of high content iron-containing opaque composites and application in 3D printing. Eurp Poly J. (in press).
20. J.T. Lin, D.C. Cheng. Modeling the efficacy profiles of UV-light activated corneal collagen crosslinking. PloS One. 2017, 12:e0175002.
21. J. T. Lin, Efficacy S-formula and kinetics of oxygen-mediated (type-II) and non-oxygen-mediated (type-I) corneal cross-linking. Ophthalmology Research. 2018, 8, 1-11.
22. J. T. Lin, K.T. Chen, D.C. Cheng, H.L. Liu, Modeling the efficacy of radical-mediated photopolymerization: the role of oxygen inhibition, viscosity and induction time. Front. Chem. 2019, 7:760. doi: 10.3389/fchem.2019.00760.
23. Lin, J.T.; Chen, K.T,; Cheng, D.C.; Liu, H.W. Modeling the efficacy of radical-mediated photopolymerization: the role of oxygen inhibition, viscosity and induction time. Front. Chem. 2019, 7:760. doi: 10.3389/fchem.2019.00760.
24. J.T. Lin, J. Lalevee, D.C. Cheng, A Critical Review for Synergic Kinetics and Strategies for Enhanced Photopolymerizations for 3D-Printing and Additive Manufacturing. Polymers, 2021, 13, 2325. https://doi.org/ 10.3390/polym13142325.
25. J.T. Lin JT, H.W. Liu, K. T. Chen , Y. C. Chiu, D.C. Cheng, Enhancing UV photopolymerization by a red-light pre-irradiation: kinetics and modeling strategies for reduced oxygen-inhibition. J Polymer Science, 2020 , 58 , 683-691 , DOI:10.1002/pol.20190201.
26. J.T. Lin, K.T. Chen, P.K. Chang, D.C. Cheng, Enhancing blue-light-initiated photopolymerization in a three-component system: kinetic and modeling of conversion strategies. J Polymer Research, 2021, 28:2.
27. J. T. Lin, K.T. Chen, D.C. Cheng, H.L. Liu, Dual-wavelength (UV and blue) controlled photopolymerization confinement for 3D-printing: modeling and analysis of measurements. Polymers, 2019, 11, 1819.
28. J. T. Lin, H.W. Liu, K.T. Chen, D.C. Cheng, 3-wavelength (UV, blue, red) controlled photopolymerization: improved conversion and confinement in 3D-printing. IEEE Access, 2020, 8, 49353-49362.